Håvard André Storvold

SES Hybrid Control

Master's thesis in Cybernetics and Robotics
Supervisor: Jan Tommy Gravdahl
June 2019

Master's thesis

NTNU
Norwegian University of Science and Technology
Faculty of Information Technology and Electrical Engineering
Department of Engineering Cybernetics

NTNU
Norwegian University of
Science and Technology

Håvard André Storvold

SES Hybrid Control

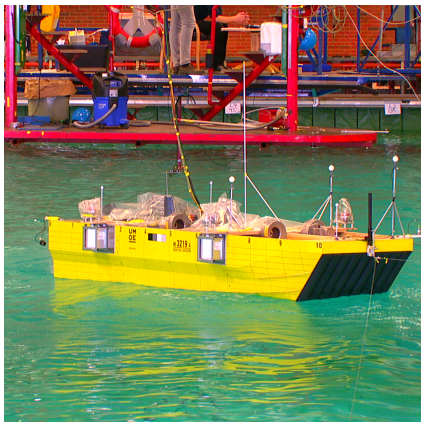

Master's thesis in Cybernetics and Robotics
Supervisor: Jan Tommy Gravdahl
June 2019

Norwegian University of Science and Technology
Faculty of Information Technology and Electrical Engineering
Department of Engineering Cybernetics

NTNU
Norwegian University of
Science and Technology

Summary

In this thesis a hybrid control system for Surface Effect Ships will be created. Hybrid control in this context refers to the mix of discrete logic, in the form of a supervisor, and continuous controllers. The system that link these two together has its origins in the project report leading to this thesis. The thesis also includes wave filtering with a Kalman filter for use in both candidate controllers and the supervisor systems. Two example uses will be detailed, the latter of which will be replicated in model testing at a basin with a wave generator.

Contributions of this thesis

This section is a summary of what work was put in by whom to make this thesis possible. Most references will be more precise when presented in the main body of the thesis.

The simulator used was provided to the author by UMOE Mandal, along with a ride control system and system matrices describing the craft. The simulator runs in simulink.

The wave filtering Kalman filter was based on work by [Fossen and Perez (1998)], but required correcting small errors in the source material, design of the wave filter itself and tuning of the Kalman filter parameters. It was also expanded to more axes and adapted to the SES input structure.

The Hybrid control system was made from scratch, however, the linear differential system of slow controller changing was introduced by [Hespana (2002)]. Hespana's tutorial also provided insight into stability, jittering concerns, and concerns regarding switching times.

The candidate controllers for part 1 were loosely based on the project report leading up to this thesis [Storvold (2018)], but were redone to use wave filtered instead of LPF filtered signals.

The candidate controllers for part 2 were from NTNU master thesises being written in parallel with this one. Their authors, Ola Mosebø Haukeland and Håkon Teigland, can be reached through [olamhaukeland@gmail.com] or [hakon.teigland@ntnu.no] respectively.

The mixing system used to blend the control signals according to supervisor input, was based on the project report leading up to this thesis [Storvold (2018)].

Importing code to LabView was done by Øyvind Auestad from UMOE, who also managed the model testing along with Vahid Hassani from Sintef/NTNU and other Sintef staff.

With these exeptions all other contents of this thesis is the original work of the author.

Preface

For the last few decades a large portion of the development of new surface effect ships has been centred in Norway, in large part at UMOE Mandal. UMOE has, because of this, collaborated with NTNU to create thesis problems and provide support for master students to finalise their degrees. This master thesis was written as a part of a masters degree at the Department of Engineering Cybernetics at NTNU and was completed in the span from January to June 2019. It would not be possible without Sintef and UMOE Mandal who conducted scale model tests of surface effect ships with a large portion of the tests dedicated to work done by master students. Lastly I would like to thank my supervisors, Professor Jan Tommy Gravdahl at NTNU and Dr. Øyvind F. Auestad at UMOE Mandal for their help.

Table of Contents

List of Figures

Abbreviations

SES	=	Surface Effect Ship
ACV	=	Air Cushion Vehicle
BCS	=	Boarding Control System
RCS	=	Ride Control System
SCC	=	Split Cushion Control
VVDP	=	Vent Valve Dynamic Positioning
CG	=	Center of gravity
CC	=	Center of air cushion
vv	=	Vent valve
PID	=	Proportional, integrating and derivative controller

Chapter 1

Introduction

In this thesis a discrete system for managing continuous controllers for a Surface Effect Ship will be developed and implemented. Both computer simulation and model testing will be used to test the system.

The Surface effect ship was developed in parallel in the U.S., USSR and in the U.K. with the U.S. based team focused on very fast military craft whereas both the U.K. and USSR teams initially produced ferries. The ferries and the experimental craft leading up to them were not nearly as fast as the US Navy's experimental craft, but were still much faster than conventional crafts of comparable size and capacity [Lavis (1991)]. While the concept of a SES ferry became more popular both Europe and South East Asia the crafts got bigger and faster and by 1991 several crafts, including those designed by Cirrus in Norway, Hovermarine in the U.K., and MTG in Germany [Lavis (1991)] could all ferry several hundred passengers at 50+ knots in calm waters.

These maximum speeds offered by SES crafts in calm sea quickly diminished in even slight to moderate seas [Lavis (1998)], or sea states 3 to 4 [WMO (2018)]. Efforts on mitigating the effect rougher seas had on the air cushion of a surface effect ship led to a wish for both more lift fan power and better ride control systems to manage this power.

For most modern surface effect ships the lift fans and associated ride control system (RCS) performs three tasks on a full scale ship:

- Eliminate acoustic resonance on the air cushion, also knows as the cobblestone effect.[Sørensen (1995)]
- Maintain a desired ride height, usually significantly higher than what buoyancy from water displacement by the hull would allow.[Auestad and T. Gravdahl (2015)]
- Reduce accelerations caused by waves passing the craft. [Auestad and T. Gravdahl

(2014)]

One of the main puropses of this is to reduce fatigue on crew and passengers which can be a major limitation to working at sea [IMO (2019)]. Earlier RCS development such as Kaplan (1981), and J. Adams (1983) were done in conjunction with the development of military prototypes by the U.S. navy. Some of the more recent work is the result of large military and civilian investments in Norway ([Auestad (2012)], [Lavis (1998)] and [Auestad and T. Gravdahl (2015)].

To perform the changes in air cushion pressure mandated by their RCS, earlier surface effect ships used variable geometry lift fans [Clark (2011)]. However, in order to provide faster actuation, air cushion pressure can be controlled by the use of vent-valves between the over-pressure of the air cushion and ambient pressure. Two vent valves, placed amidships, one on each side, was used by Bua and Varmåk Bua and Vamråk (2016) to produce lateral movement of a scale SES, inspired by the Umoe Mandal Wave Craft series. This lead to modelling of a surface effect ship with four vent valves, and the subsequent cushion force modelling and control work done in the project report leading up to this thesis [Storvold (2018)]. The report shows simulation results that suggests simultaneous sway, yaw and heave control is possible, but will suffer from having to share actuator allocations.

Figure 1.1: A UMOE mandal Wavecraft render

Current effort by UMOE Mandal include a ”split cushion” concept, this could in theory allow for control of up to 5 axis, (sway, heave, pitch, roll and yaw). In order to let the different controllers work in conjunction with each controller having adequate access to the actuators a supervisory system was suggested.

As described by [Hespana (2002)], supervisory control is the combination of logical decision making and a continuous system. This is often implemented using discrete logic to act upon a bank of continuous controllers, resulting in a hybrid control system, where the word ”hybrid” refers to the combination of discrete and continuous signals.

Wave filtering is a commonly used tool for reducing actuator usage in marine systems often through usage of a Kalman filter [Fossen and Perez (1998)]. Earlier experiences with SES control [Storvold (2018)] have suggested that wave filtering could provide benefits when encountering actuator saturation.

Chapter 2

Vessel model

This chapter, summarises the model of the craft as handed over by UMOE Mandal, as well as work done in the project report leading up to this thesis, as described in sections [ref to prevlit]. The basis of the model is the general marine system model and the notation found in (Fossen (2011)) with symbols as follows:

Symbol	Formula	Description
η	$\dot{\eta} = J_b^n(\theta_{nb})\nu$	Position $\eta = [n, e, d, \theta, \phi, \psi]$ NED-frame
ν	-	Velocity in body frame
ν_c	-	Velocity of the water current
ν_r	$\nu - \nu_c$	Velocity relative to the current
μ	$\dot{\mu} = A_m\mu + B_m\nu_r$	Fluid memory variable
M	$= M_{RB} + M_A$	Total mass, vessel + added
B_ν	-	Linear viscous damping
$B_{\nu 2}$	-	Quadratic viscous damping
$g(\eta)$	-	Gravity and buoyancy
$g(\eta)$	-	Gravity and buoyancy

Table 2.1: Table of symbols

The coordinate system used to describe the body frame in this thesis is defined as follows: Origin in the centre of gravity, x-axis along the centerline in the forward direction of the vessel, z-axis downwards, and y-axis toward starboard to complete the right hand system.

2.1 Dynamic equation

The model, based on the general marine system model,

$$M\dot{\nu} + B_\nu \nu_r + B_{\nu 2}\nu_r|\nu_r| + \mu + g(\eta) = \tau_{env} - \tau_{cush}, \tag{2.1}$$

$$\dot{\eta} = J_b^n(\theta_{nb})\nu$$

neglects terms such as Coriolis and centripetal forces, and simplifies τ_{env} to τ_{wave} which only includes waves. The model also assumes that the main propulsion, typically water jets, is disabled.

Parts of the model was calculated by use of ShipX(Veres) and the MSS toolbox [Fossen and Perez (2004)], on a 3D ship model. It should be noted that the model is based on the ship remaining close to standard draught, as such large fluctuations in draught will result in inaccurate hydrodynamics.

2.2 Air cushion dynamics

Symbol	Formula	Description
p_c	$p_a + p_u(i,t)$	Pressure in the air cushion
p_a	-	Ambient pressure
$p_u(i,t)$	-	Excess pressure in air cushion number i
p_0	-	Equilibrium cushion pressure
A_L	$A_{L_{active}} + A_{L_{passive}}$	Effective air leak area
$A_{L_{active}}(vv_{pos})$	Equation 2.3	Effective air leak area at vent valve
$A_{L_{passive}}$	-	Passive leak area
ρ_a	$1,25\mathrm{kg/m}^3$	Density of air
ρ_a	-	Equilibrium cushion pressure
Q_{in}	-	Air flow from lift fans
Q_{out}	$= c_n A_L \sqrt{2p_u/\rho_a}$	Total mass, vessel + added
$(x_{vv}(i), y_{vv}(i))$	-	Position of vent valve number i
$(x_c(i), y_c(i))$	-	Position of cushion number i
$A_c(i)$	-	Area under cushion number i
c_n	-	Loss factor in vent valves

Table 2.2: Table of symbols

For this thesis to include both a case where the air cushion is split and one where it is not, it needs two models for the air cushion(s). This can be done by expanding [Storvold (2018)] to include the case of the split air cushion. For this section the forces from the

cushion's pressure and the thrust forces from the escaping air will be looked at separately, as $\tau_{cush(P)}$ and $\tau_{cush(T)}$ respectively. This gives:

$$\tau_{cush} = \begin{cases} \tau_{1cush} = \tau_{1cush(P)} + \tau_{1cush(T)} & \text{In case: Single cushion} \\ \tau_{4cush} = \tau_{4cush(P)} + \tau_{4cush(T)} & \text{In case: Split cushion} \end{cases} \tag{2.2}$$

Where

$$A_{L_{active}} = \sum_{valves} \frac{A_{L_{MAX}}}{100}(C_{vv2}{vv_{pos}}^2 + C_{vv1}vv_{pos} + C_{vvc}), \tag{2.3}$$

and $A_{L_{MAX}}$ is given by the producer of the vent valve, and the polynomial coefficients were found by UMOE Mandal by use of curve fitting to test data [UMOE-Mandal (2019)].

2.3 Air cushion pressure forces

The forces created by air escaping the cushion can be modelled using two basic assumptions, the air within the cushion has, on average, the same velocity as the craft, and the air escaping through leaks not within vent valves produces a near zero net force. For the case where the craft has a single air cushion, calculations from [Storvold (2018)] can be used. However, the amplitude of the forces can still be calculated with a similar method.

$$|F_{pressure}| = A_c(i)p_u(i,t) \tag{2.4}$$

2.3.1 Single cushion

For the case where the craft has a single air cushion the force could be assumed to be along the crafts z-axis and thus providing no torque.

$$\tau_{1cush(P)} = \begin{bmatrix} 0 \\ 0 \\ -A_c(i)p_u(1,t) \\ 0 \\ 0 \\ 0 \end{bmatrix} \tag{2.5}$$

2.3.2 Split cushion

For the case where the craft has a air cushion split into four parts the force could be assumed to be parallel to the crafts z-axis, but with an offset denoted by $(x_c(i), y_c(i))$.

$$\tau_{4cush(P)} = \begin{bmatrix} 0 \\ 0 \\ \sum_{i=1}^{n} -A_c(i)p_u(i,t) \\ \sum_{i=1}^{n} A_c(i)p_u(i,t)y_c(i) \\ \sum_{i=1}^{n} A_c(i)p_u(i,t)x_c(i) \\ 0 \end{bmatrix} \tag{2.6}$$

2.4 Air cushion thrust forces

$$|F_{thrust}| = \frac{2c_n^2}{A_{Lmax}} A^2_{L_{active}}(i,t)p_u(i,t) \tag{2.7}$$

For the thrust forces, splitting the air cushion does not charge the direction of the produced forces, but from the equation above, each vent valve has a different pressure potential in the case of a split cushion.

2.4.1 Single cushion

$$\tau_{1cush(T)} = \begin{bmatrix} 0 \\ \sum_{i=1}^{n} -\frac{2c_n^2}{A_{Lmax}} A^2_{L_{active}}(i,t)p_u(1,t)sign(y_{vv}(i)) \\ 0 \\ 0 \\ 0 \\ \sum_{i=1}^{n} \frac{2c_n^2}{A_{Lmax}} A^2_{L_{active}}(i,t)p_u(1,t)x_{vv}(i)sign(y_{vv}(i)) \end{bmatrix} \tag{2.8}$$

2.4.2 Split cushion

$$\tau_{4cush(T)} = \begin{bmatrix} 0 \\ \sum_{i=1}^{n} -\frac{2c_n^2}{A_{Lmax}} A^2_{L_{active}}(i,t)p_u(i,t)sign(y_{vv}(i)) \\ 0 \\ 0 \\ 0 \\ \sum_{i=1}^{n} \frac{2c_n^2}{A_{Lmax}} A^2_{L_{active}}(i,t)p_u(i,t)x_{vv}(i)sign(y_{vv}(i)) \end{bmatrix} \tag{2.9}$$

Note that the only difference between the two cases is the fact that the single cushion case all vent valves pull from the same pressure vessel.

2.5 Total cushion force

2.5.1 Single cushion

$$\tau_{1cush} = \begin{bmatrix} 0 \\ \sum_{i=1}^{n} -\frac{2c_n^2}{A_{Lmax}} A_{L_{active}}^2(i,t) p_u(1,t) sign(y_{vv}(i)) \\ -A_c(i) p_u(1,t) \\ 0 \\ 0 \\ \sum_{i=1}^{n} \frac{2c_n^2}{A_{Lmax}} A_{L_{active}}^2(i,t) p_u(1,t) x_{vv}(i) sign(y_{vv}(i)) \end{bmatrix} \tag{2.10}$$

2.5.2 Split cushion

$$\tau_{4cush(T)} = \begin{bmatrix} 0 \\ \sum_{i=1}^{n} -\frac{2c_n^2}{A_{Lmax}} A_{L_{active}}^2(i,t) p_u(i,t) sign(y_{vv}(i)) \\ \sum_{i=1}^{n} -A_c(i) p_u(i,t) \\ \sum_{i=1}^{n} A_c(i) p_u(i,t) y_c(i) \\ \sum_{i=1}^{n} A_c(i) p_u(i,t) x_c(i) \\ \sum_{i=1}^{n} \frac{2c_n^2}{A_{Lmax}} A_{L_{active}}^2(i,t) p_u(i,t) x_{vv}(i) sign(y_{vv}(i)) \end{bmatrix} \tag{2.11}$$

Chapter 3

Continuous controllers

In the project report leading up to this thesis [Storvold (2018)] a mixing system for combining several controllers in a surface effect ship was made. In the following section that system will be adapted to supervisory control, with subsequent sections describing new candidate controllers.

3.1 Mixing

While the supervisor itself will be presented in chapter six, this section will assume that a vector σ of size m, where m is the number of candidate controllers, containing non-negative scaling factors will be produced by the supervisor. The column vectors produced by each candidate controller will be concatenated as follows

$$\boldsymbol{u_{concat}} = [u_1 u_2 ... u_m].$$

The mixing system will also scale the outgoing signal to fit within minimum and maximum actuator limits. In this scenario, vv_{min} and vv_{max}, respectively.This while varying about the To implement this, the available actuator space will be denoted as

$$\alpha = min(vv_{max} - vv_{bias}, vv_{bias} - vv_{min}) \tag{3.1}$$

$$u_{tot} = (\sigma \boldsymbol{u_{concat}^T})^T \tag{3.2}$$

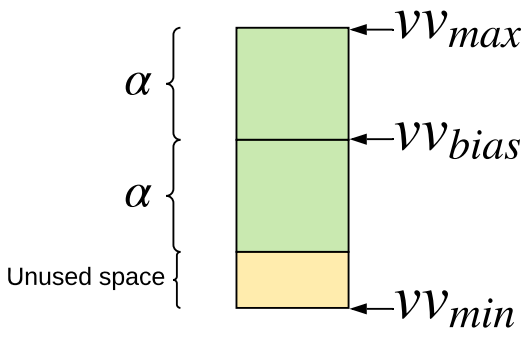

Figure 3.1: Availible actuator space

$$vv_{cmd} = \frac{\alpha \cdot u_{tot}}{max(|u_{tot1}|, |u_{tot2}|, ..., |u_{totn}|, \alpha)} \tag{3.3}$$

3.2 Controllers for single cushion operation

To test the basic principles of hybrid control, some PID controllers were created.

$$u_1 = K_{p_{sway}}\epsilon_{sway} + K_{i_{sway}}\int_0^t \epsilon_{sway} + K_{d_{sway}}\nu_{sway} \tag{3.4}$$

$$u_2 = RCS(\dot{\nu}_{heave}) \tag{3.5}$$

$$u_3 = K_{p_{yaw}}\epsilon_{yaw} + K_{i_{yaw}}\int_0^t \epsilon_{yaw} + K_{d_{yaw}}\nu_{yaw} \tag{3.6}$$

However, the error signals will be based on wave filtered measurements produced by a filter presented in the next chapter.

$$\epsilon_{sway} = \hat{\eta}_{sway} - ref_{sway} \tag{3.7}$$

$$\epsilon_{yaw} = \hat{\eta}_{yaw} - ref_{yaw} \tag{3.8}$$

$$\tag{3.9}$$

3.3 Controllers for split cushion operation

For split cushion operation premade candidate controllers are used. The RCS remains from the previous section but two new controllers are introduced.

Roll and pitch control will be done by a controller described in a currently in progress master thesis by Ola Mosebø Haukeland [olamhaukeland@gmail.com] and will not be disclosed in this thesis. It produces separate control signals for roll and pitch that will be used separately in this thesis. For the purpose of this thesis the controller will be called the split cushion control system, or SCC.

Sway and yaw will be controller by a system based on dynamic positioning described in a currently in progress master thesis by Håkon Teigland [hakon.teigland@ntnu.no] and will not be disclosed in this thesis. It produces a single control signal for both sway and yaw and is called the Vent Valve Dynamic Positioning system, or VVDP.

$$u_1 = SCC_{roll}(\nu, \epsilon_{roll}) \tag{3.10}$$
$$u_2 = SCC_{pitch}(\nu, \epsilon_{pitch}) \tag{3.11}$$
$$u_3 = RCS(\dot{\nu}_{heave}) \tag{3.12}$$
$$u_4 = VVDP(\nu, \epsilon_{sway}, \epsilon_{yaw}) \tag{3.13}$$

Chapter 4

Observer

As discussed in section 3, wave filtered position and attitude measurements are needed to drive the controller library. This can be done using a Kalman filter and second order linear filters. One method for doing this was described in [Fossen and Perez (1998)], based on a dynamic vessel model very similar to the one used in this thesis.

It is based on a linear model and a second order wave filter on the form

4.1 Wave filter

$$G(s) = \frac{\omega_0^2 s}{s^2 + 2\lambda_n \omega_0 s + \omega_0^2}, \tag{4.1}$$

for state n. This filter will be implemented as a linear time invariant state space based on a constant wave frequency ω_0. Letting the filters internal state vector be called ξ, the filtered wave frequency state vector be called η_{WF}, and the filtered low frequency state vector be called η_{LF}.

$$\dot{\boldsymbol{\xi}} = \boldsymbol{A}_\omega \boldsymbol{\xi} + \boldsymbol{E}_\omega w \tag{4.2}$$
$$\boldsymbol{\eta}_{wf} = \boldsymbol{C}_\omega \boldsymbol{\xi} \tag{4.3}$$

Using this we can define $\boldsymbol{\eta}_{lf}$, the filtered signal to be used for LF control, by:

$$\boldsymbol{y} = \boldsymbol{\eta}_{lf} + \boldsymbol{\eta}_{wf} + \boldsymbol{v} \tag{4.4}$$

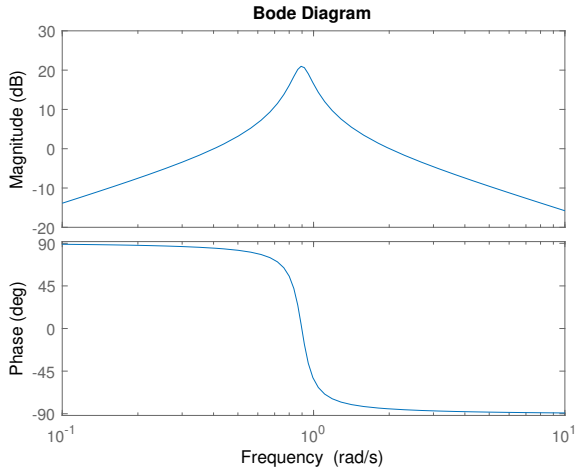

Figure 4.1: Wave filter

Where v is a measurement noise vector that will not be included in the simulation. This will result in each of the vessels axis having a corresponding filter matrix on the form:

$$\boldsymbol{G}_n = \begin{bmatrix} 0 & 1 \\ -\omega_0^2 & -2\lambda_n\omega_0 \end{bmatrix}. \tag{4.5}$$

4.2 Wave filter state space

The filter submatrixes can be combined into the A_w from equation 4.2.

$$\boldsymbol{A}_\omega = \begin{bmatrix} \boldsymbol{G}_1 & \boldsymbol{0}_{2\times2} & \dots & \boldsymbol{0}_{2\times2} \\ \boldsymbol{0}_{2\times2} & \boldsymbol{G}_2 & \ddots & \vdots \\ \vdots & \ddots & \ddots & \boldsymbol{0}_{2\times2} \\ \boldsymbol{0}_{2\times2} & \dots & \boldsymbol{0}_{2\times2} & \boldsymbol{G}_6 \end{bmatrix} \tag{4.6}$$

Lastly, in order to match the filter specified in equation 4.1, the noise matrix is formed by diagonally combining 1x2 submatrixes in a manner similar to the above matrix.

$$\boldsymbol{E_\omega} = \begin{bmatrix} 0 & 0 & \dots & 0 \\ \omega_0^2 & 0 & \dots & 0 \\ 0 & 0 & \dots & 0 \\ 0 & \omega_0^2 & \ddots & \vdots \\ \vdots & \ddots & \ddots & 0 \\ \vdots & \ddots & \ddots & 0 \\ 0 & \dots & 0 & 0 \\ 0 & \dots & 0 & \omega_0^2 \end{bmatrix} \tag{4.7}$$

The output matrix from equation 4.3 is then realised to form the filter.

$$\boldsymbol{C_w} = \begin{bmatrix} 0 & 1 & 0 & 0 & \dots & 0 & 0 \\ 0 & 0 & 0 & 1 & \ddots & \vdots & \\ \vdots & & \ddots & & \ddots & 0 & 0 \\ 0 & 0 & \dots & 0 & 0 & 0 & 1 \end{bmatrix} \tag{4.8}$$

4.3 Kalman filter state space

These can be combined into the system matrices of the linearised system to form $\boldsymbol{A}$, $\boldsymbol{B}$, $\boldsymbol{E}$ and $\boldsymbol{H}$ for the following state space.

$$\dot{\boldsymbol{x}} = \boldsymbol{A}\boldsymbol{x} + \boldsymbol{B}\boldsymbol{u} + \boldsymbol{E}\boldsymbol{w} \tag{4.9}$$
$$\boldsymbol{y} = \boldsymbol{H}\boldsymbol{x} + v \tag{4.10}$$

From linearising equation 2.1, we find the following matrices:

$$\boldsymbol{A} = \begin{bmatrix} \boldsymbol{A}_\omega & \boldsymbol{0}_{12\times6} & \boldsymbol{0}_{12\times6} & \boldsymbol{0}_{12\times6} \\ \boldsymbol{0}_{6\times12} & \boldsymbol{0}_{6\times6} & \boldsymbol{0}_{6\times6} & \boldsymbol{I}_{6\times6} \\ \boldsymbol{0}_{6\times12} & \boldsymbol{0}_{6\times6} & \boldsymbol{0}_{6\times6} & \boldsymbol{0}_{6\times6} \\ \boldsymbol{0}_{6\times12} & \boldsymbol{0}_{6\times6} & \boldsymbol{M}^{-1} & -\boldsymbol{M}^{-1}\boldsymbol{D} \end{bmatrix} \tag{4.11}$$

$$\boldsymbol{B} = \begin{bmatrix} \boldsymbol{0}_{12\times6} \\ \boldsymbol{0}_{6\times6} \\ \boldsymbol{0}_{6\times6} \\ \boldsymbol{M}^{-1}\boldsymbol{B}_u \end{bmatrix} \tag{4.12}$$

$$\boldsymbol{E} = \begin{bmatrix} \boldsymbol{E_\omega} \\ \boldsymbol{0}_{6\times6} \\ \boldsymbol{I}_{6\times6} \\ \boldsymbol{M}^{-1} \end{bmatrix} \tag{4.13}$$

$$\boldsymbol{H} = \begin{bmatrix} \boldsymbol{C_\omega} & \boldsymbol{I}_{6\times6} & \boldsymbol{0}_{6\times6} & \boldsymbol{0}_{6\times6} \end{bmatrix} \tag{4.14}$$

To generate the input u, equations 2.10 and 2.11 were linearized about the vessels average draught on lift.

4.4 Discretization and implementation

In order to implement the filter it was disretized using the MATLAB c2d function. This provides an exact discetization assuming staircase inputs using zero order hold. R and Q were set as diagonal matrixes and the Kalman filter was implemented as follows:

```
K = P_*H'*(H*P_*H' + R)^-1;
xHat = x_ + K*(y - H*x_);
P_ = (eye(30) - K*H)*P_;
x_ = A*xHat + B*u;
P_ = A*P_*A' + Q;
```

4.5 Results

After running several simulations to tune the Kalman filter parameters, a simulation of the open loop system with 2.5m waves with a 7 second period yielded the following result for the surge and sway axes:

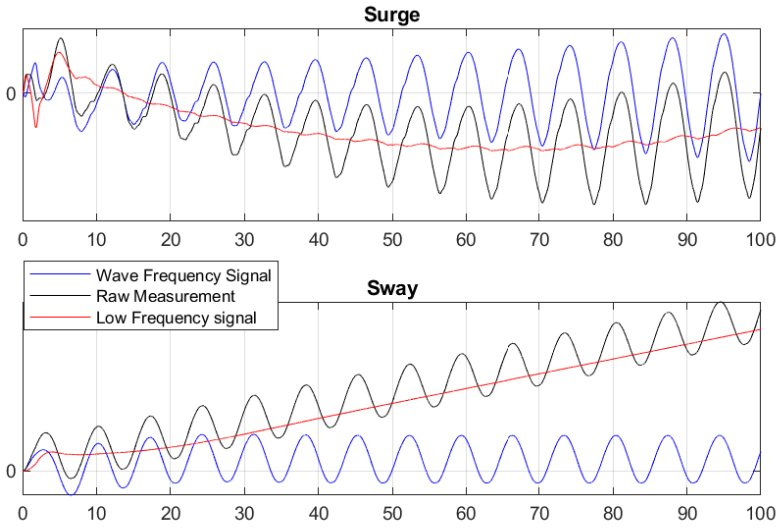

Figure 4.2: Surge and sway movement filtered into two seperate signals

Chapter 5

Supervisory Control

In this thesis hybrid control will be implemented by adding a supervisor on top of other controllers. This can be done by altering the input vector to the linear mixing system, shown as σ in the figure below.

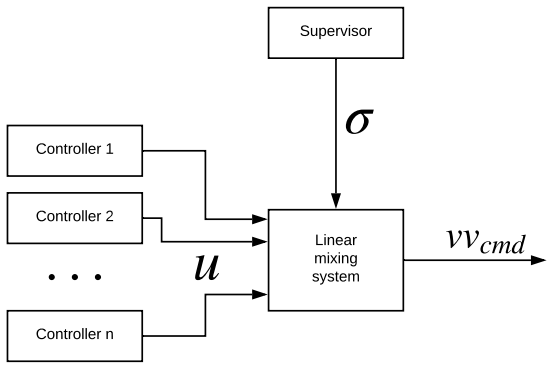

Figure 5.1: Supervisor

5.1 Controller bank

For more traditional hybrid control systems there is more than one controller per control axis, often several controllers for only a single controlled variable [Hespana (2002)]. Because of the linear mixing system used in this thesis the output can be a mix of any number of controllers regardless of their respective control axis. However, as seen in [Storvold

(2018)], one can easily run into severe saturation issues when mixing many controllers.

In order to implement this, one can predefine σ vectors that has at least one zero element. This will let the system designer specify a wanted behaviour in a number of control axis without having many controllers active in a very limited actuator space.

5.2 Switching logic

These predefined σ vectors each need to match at least one condition defined by the switching logic. This can be done using multi-estimators, a state machine or simple if-, else-if- and else- statements. In this thesis the latter will be used as an example, however, some assumptions will have to be made.

There must be exactly one controller defined as the default and then the other controllers implemented as follows:

```
if([condition_1]):
    reference_controller = predef_sigma_1
else if([condition_2]):
    reference_controller = predef_sigma_2
else:
    reference_controller = default_sigma
```

With this implementation overlapping conditions will be prioritised by their order. Though, nonoverlapping conditions without complex shapes or narrow gaps will give fewer changes along smooth trajectories. In general, if the absolute value of the curvature of the trajectory is less than the minimum absolute value of the curvature of the conditions edge the frequency of intersections will be bounded. However, this condition severely limits the size and shapes a condition area can have.

5.3 Switching times and smoothness

In order to accept any combination of conditions, the system needs to be able to handle any number of changes of condition per unit of time. However, the system should not be able to enter a state where it constantly produces drastic and fast changes in control inputs, a state called jittering. To do this, anti-jittering tools have been used.

5.3.1 Dwell time

The simplest means of limiting the frequency at which the controller output can change is to set a hard cap, or inversely, a lower limit for time between changes. This limit, denoted

T_D, is in [Hespana (2002)] also shown to be the maximum time-span in which the supervisor has a disparity between condition and controller selection. It is also worth considering how long any controller will take to produce a measurable effect on the variables evaluated as parts of the conditions and to have the dwell time be longer than that to ensure that some effect is generated by the active controller during its minimum run time.

5.3.2 Smooth switching

To facilitate smooth switching we establish two different controllers, one reference and one for output. The output will lag behind the reference as a stable linear differential system.

$$\dot{\sigma}_{out} = -\frac{1}{T_C}(\sigma_{out} - \sigma_{ref}) \tag{5.1}$$

For time step k and an update frequency of f_s this was discretisied as:

$$\sigma_{out}(k) = (1 - e^{\frac{f_s}{T_C}})\sigma_{out}(k-1) + e^{\frac{f_s}{T_C}}\sigma_{ref}(k) \tag{5.2}$$

As will be seen later T_C is a very powerful tuning parameter, in this thesis two different cases will be demonstrated: $T_C << T_D$ and $T_C >> T_D$. The first case is the simplest, in that case only in brief transition periods will there ever be a σ_{out} that is not a member of the predefined set. Additionally, the σ_{out} vector will only ever be a linear combination of maximum two predefined σ vectors.

However in the second case, $T_C >> T_D$, the supervisors σ_{out} can stabilise on a linear combination of several predefined σ vectors. This will let the supervisor mimic a continuous adaptive system when close to condition borders, at the cost of slow operation when transitioning through conditions.

5.4 Hybrid controller - Single Cushion

In order to test the system two example Hybrid control systems will be created, one for single cushion and one for split cushion operation. For the single cushion case the setup consists of a set of limits and priorities as follows.

1. The heading (yaw position) should be within a given threshold.
2. The sway position should be within a given threshold.
3. Heave dampening should be done whenever possible

Along with these conditions a controller bank was created, where each condition matches the controller with the same number.

1. Only yaw control
2. Only sway control
3. Only heave dampening

5.5 Hybrid controller - Split Cushion

To test the hybrid systems behaviour in more complex scenarios, a system with more control axes and nonlinear controllers from chapter 3 is used.

One of the purposes of the split cushion is to better dampen more wave frequency movements, and as such the supervisor should monitor these. This will be implemented using a pseudo RMS value γ for variable n calculated as:

$$\gamma_n(k) = \sqrt{\frac{T_\gamma f_s}{T_\gamma f_s + 1}\gamma_n(k-1)^2 + \eta_{WF}(n)^2} \tag{5.3}$$

Using the signals a new set of conditions and controllers was created based on the following rule: If the heave RMS is over a threshold, dampen it, along with either pitch or roll, whichever's RMS is highest. Otherwise, is the heave RMS is below the threshold, do pure DP sway/yaw control.

1. Heave RMS (γ_{heave}) is over the threshold and $\gamma_{roll} > \gamma_{pitch}$
2. Heave RMS (γ_{heave}) is over the threshold and $\gamma_{roll} < \gamma_{pitch}$
3. DP sway and yaw control

Along with these conditions a controller bank was created, where each condition matches the controller with the same number.

1. Heave and roll dampening
2. Heave and pitch dampening
3. DP only

These example conditions and controller combinations are implemented in matlab function blocks in Simulink to be part of the simulations in the following chapter.

Chapter 6

Simulation results

With the hybrid control system, candidate controllers and mixing system implemented into the Simulink diagram provided by UMOE Mandal. Simulink ran using the following settings; fixed 0,005s step size, ode3 (Bogack-Shampine) solver as suggested by Simulinks automatic solver selection. All plots were generated using the timeseries format and the Matlab plot function. The tests conducted had parameters set by the tables at the start of each of the following sections. Parameters that remained unchanged throughout both tests can be found below. The y axis of most plots are anonymised in order to protect UMOE Mandal. The scaling and limits are kept the same throughout each set of runs for ease of comparisons.

Parameter	Symbol	Value
Dwell time	T_D	10s
Pseudo RMS time constant	T_γ	25s

Table 6.1: Table of test parameters

6.1 Single cushion

Run number	Wave direction	Wave height	Wave period	T_C
1	0°	1,5m	5s	5s
2	0°	2,5m	7s	5s
3	0°	2,5m	7s	50s
4	45°	1,5m	5s	5s
5	45°	2,5m	7s	5s
6	45°	2,5m	7s	50s
7	90°	1,5m	5s	5s
8	90°	2,5m	7s	5s
9	90°	2,5m	7s	50s

Table 6.2: Table of simulation parameters single cushion

Note: The runs with $T_C = 50s$ will have a longer run time Conditions give the following controllers:

1. Only yaw control
2. Only sway control
3. Only heave dampening

6.1.1 Run 1

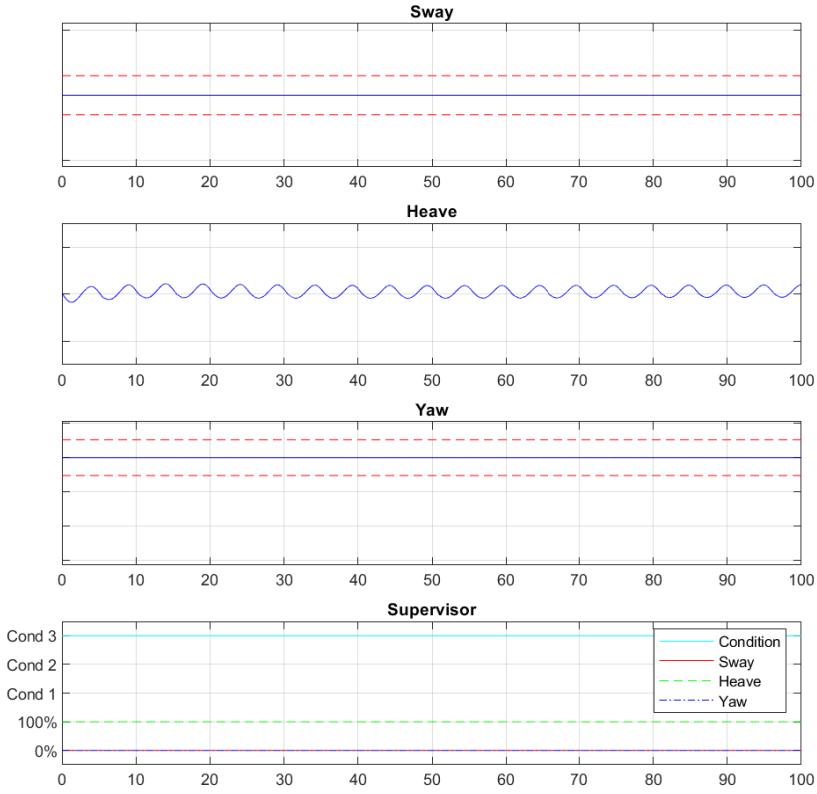

Figure 6.1: Simulation run 1

6.1.2 Run 2

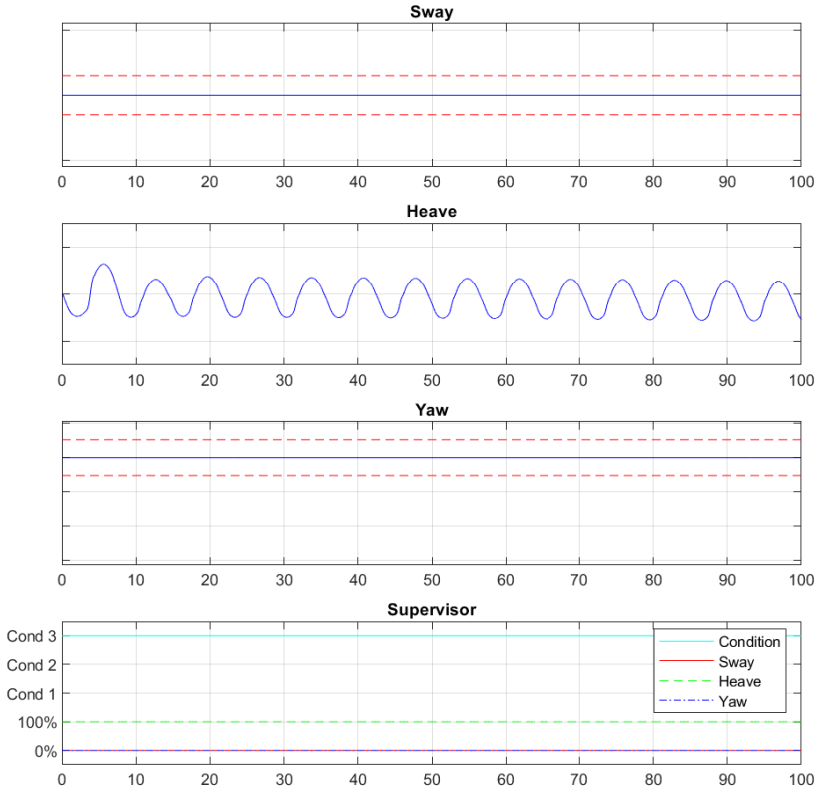

Figure 6.2: Simulation run 2

6.1.3 Run 3

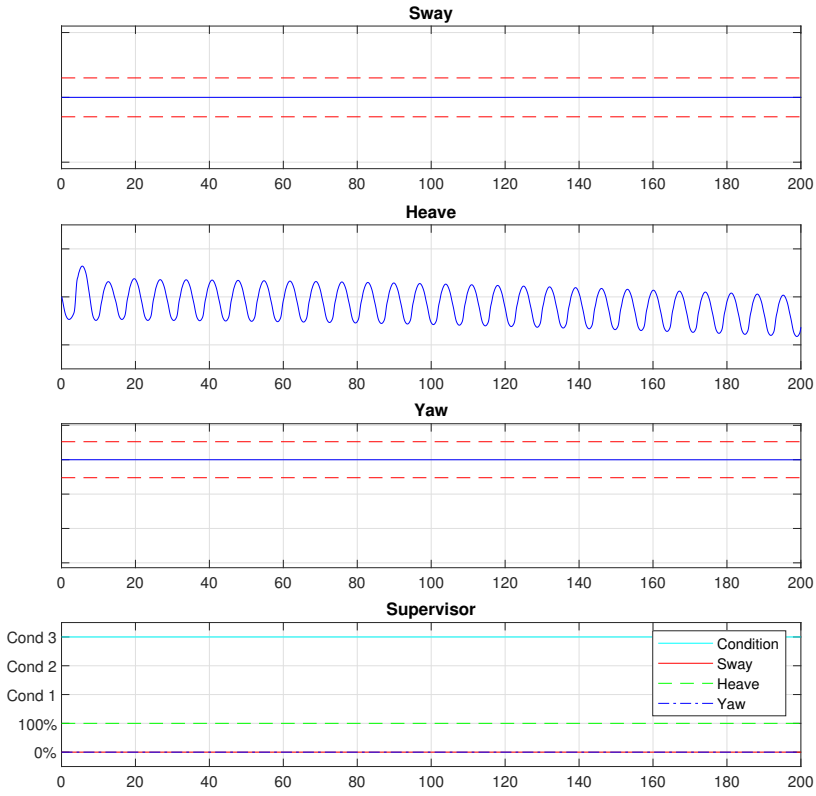

Figure 6.3: Simulation run 3

6.1.4 Run 4

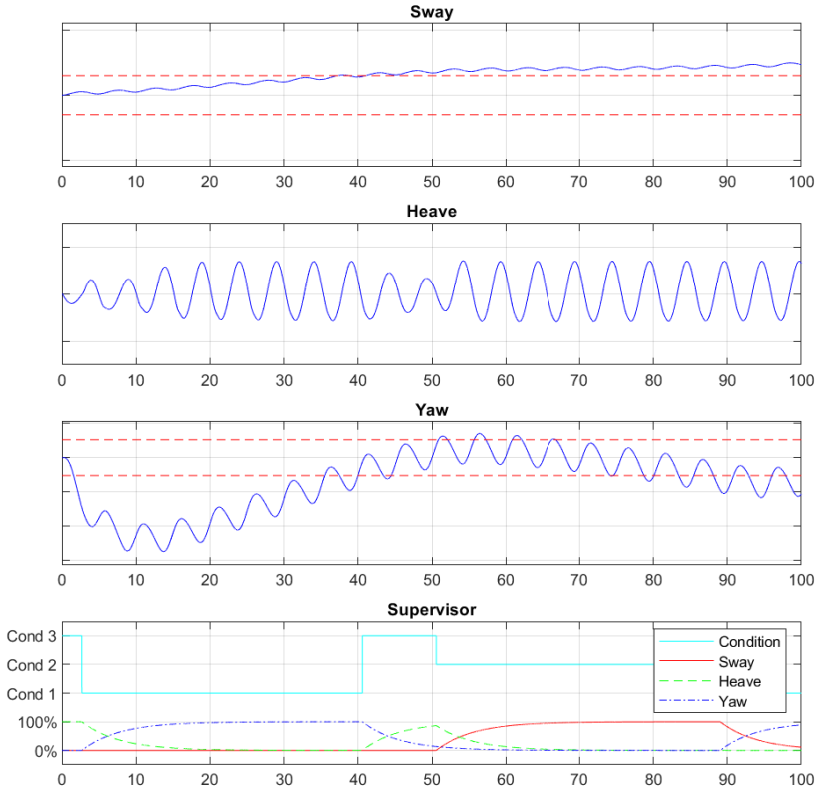

Figure 6.4: Simulation run 4

6.1.5 Run 5

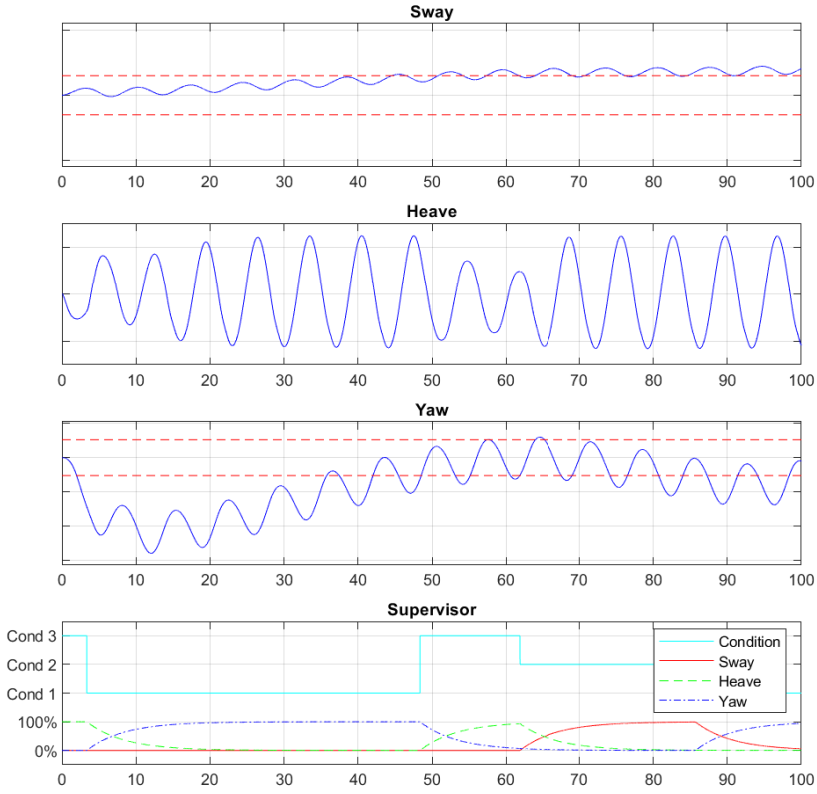

Figure 6.5: Simulation run 5

6.1.6 Run 6

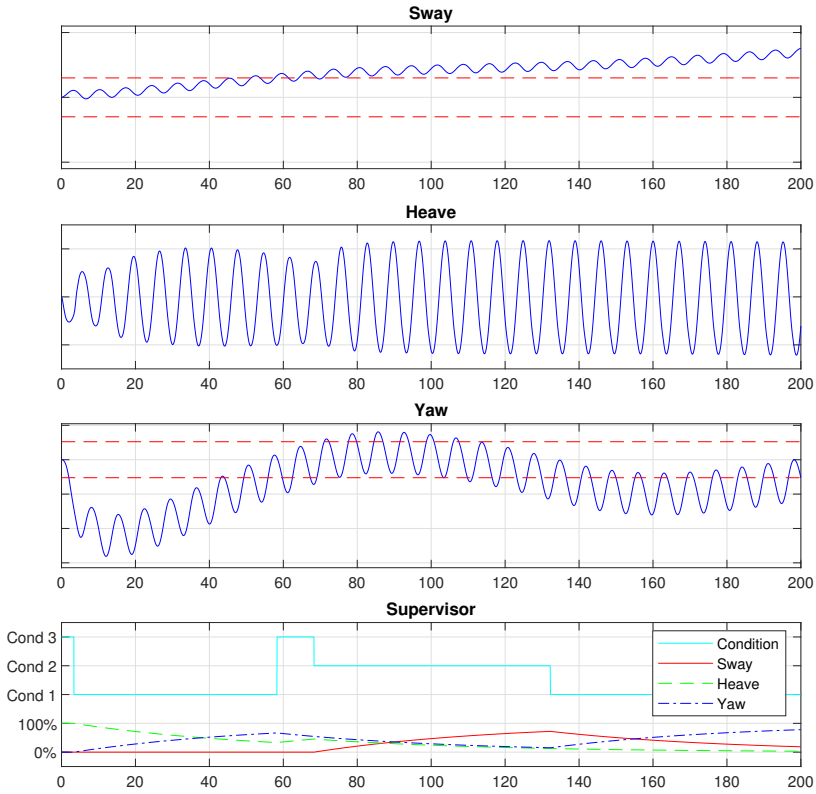

Figure 6.6: Simulation run 6

6.1.7 Run 7

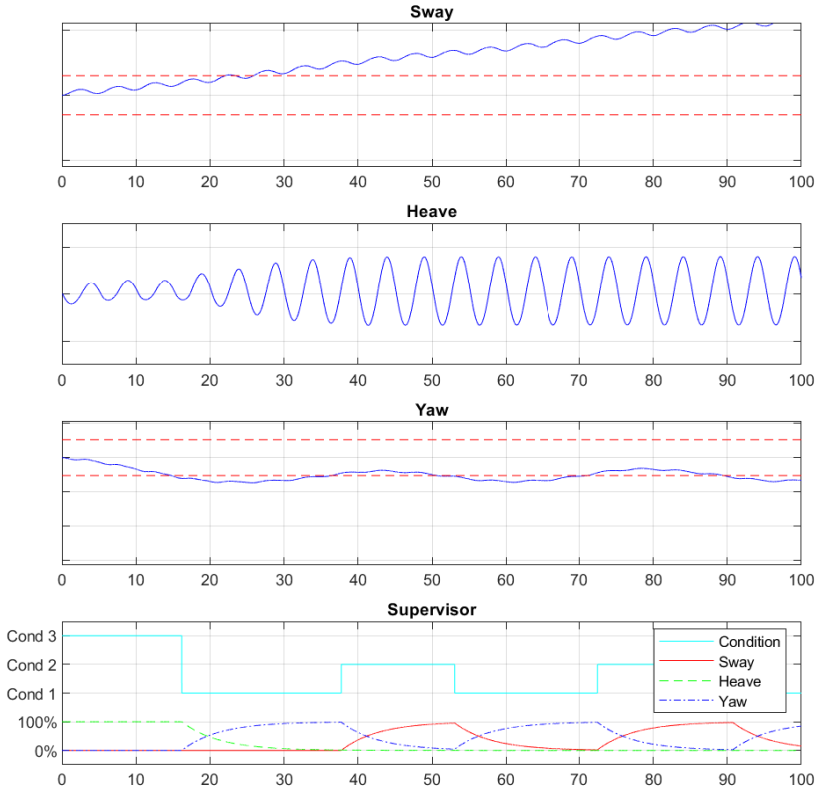

Figure 6.7: Simulation run 7

6.1.8 Run 8

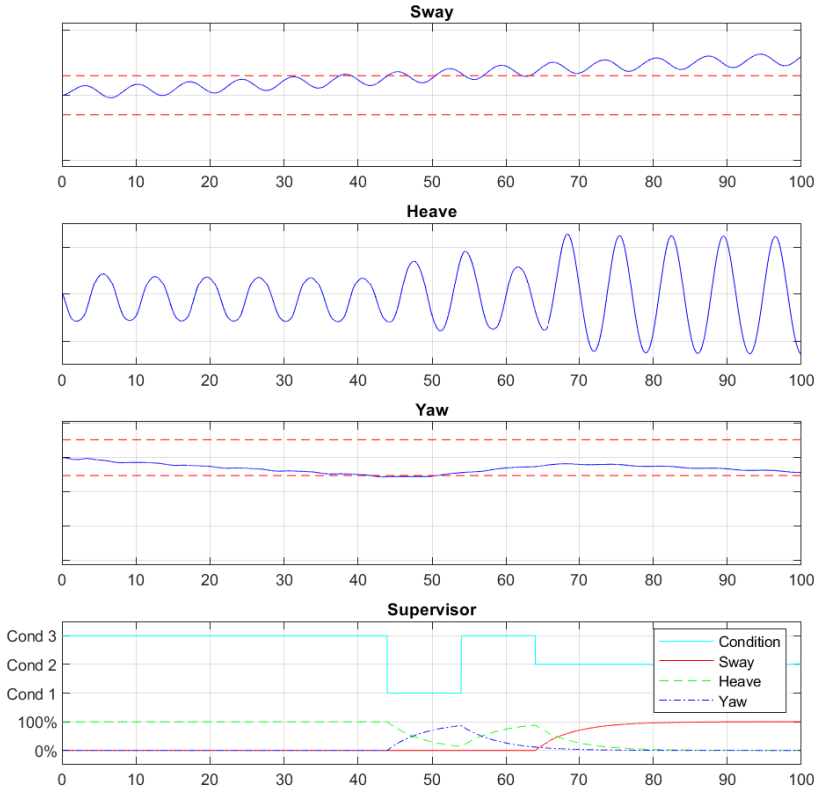

Figure 6.8: Simulation run 8

6.1.9 Run 9

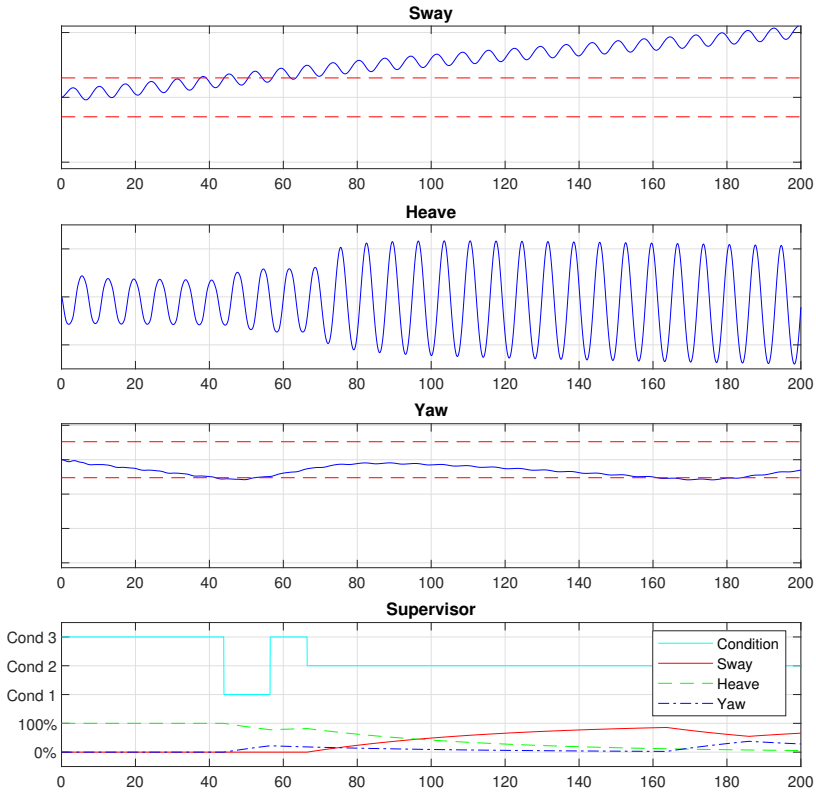

Figure 6.9: Simulation run 9

6.2 Split cushion

Run number	Wave direction	Wave height	Wave period	T_C
1	0°	1,5m	5s	5s
2	0°	2,5m	7s	5s
3	0°	2,5m	7s	50s
4	45°	1,5m	5s	5s
5	45°	2,5m	7s	5s
6	45°	2,5m	7s	50s
7	90°	1,5m	5s	5s
8	90°	2,5m	7s	5s
9	90°	2,5m	7s	50s

Table 6.3: Table of simulation parameters split cushion

Note: The runs with $T_C = 50s$ will have a longer run time Conditions give the following controllers:

1. Heave and roll dampening
2. Heave and pitch dampening
3. DP only

6.2.1 Run 1

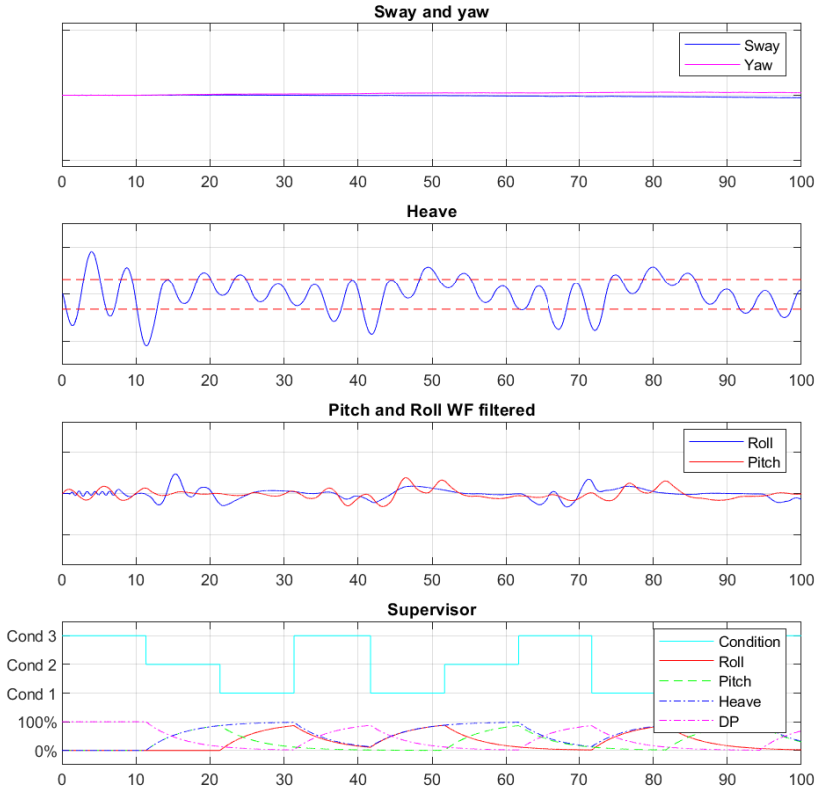

Figure 6.10: Simulation run 1

6.2.2 Run 2

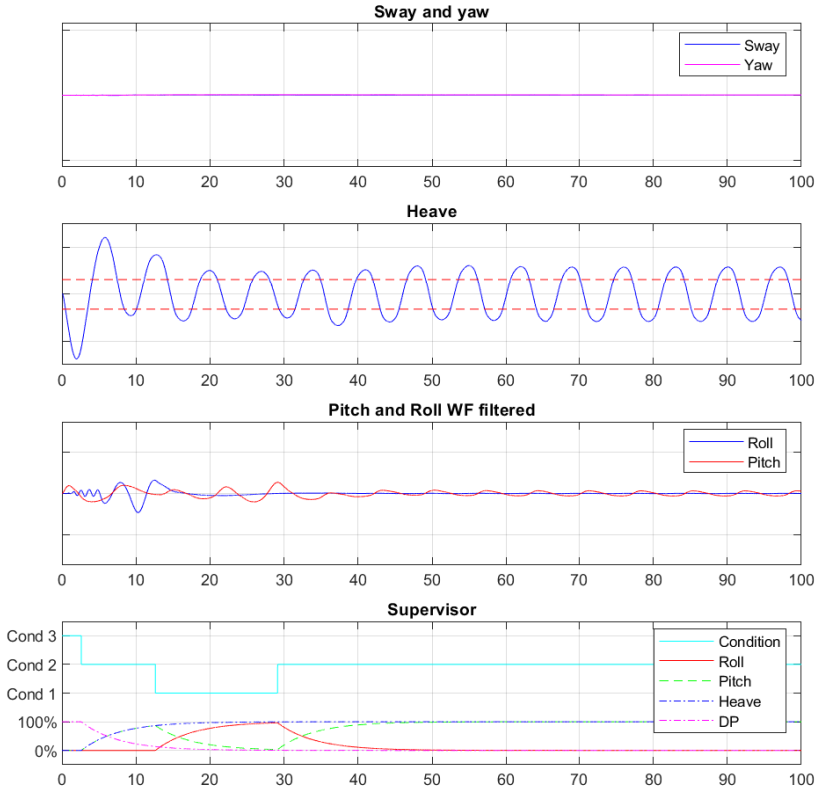

Figure 6.11: Simulation run 2

6.2.3 Run 3

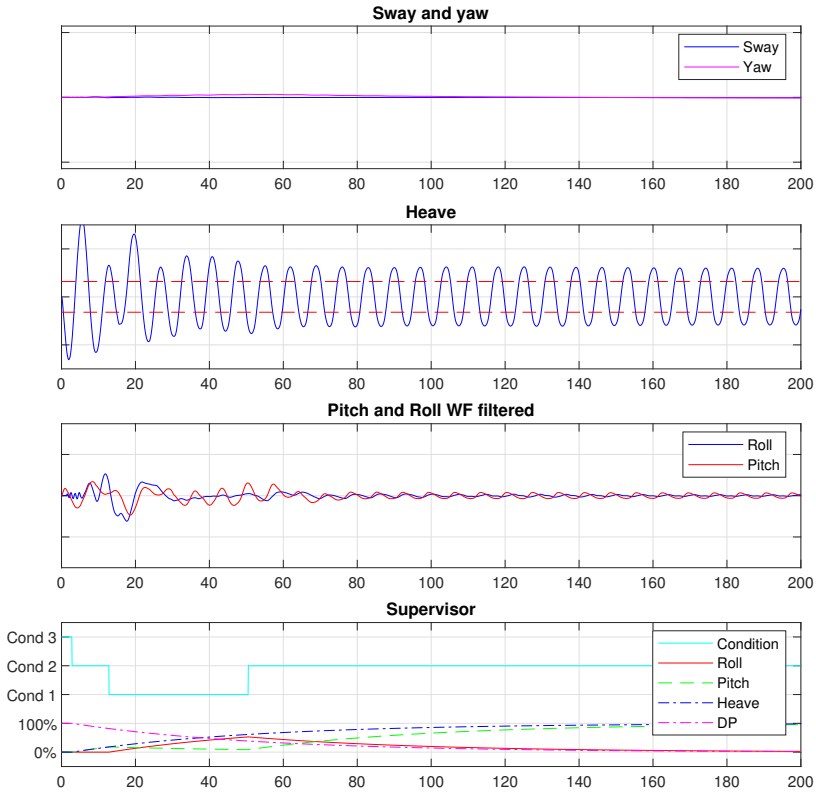

Figure 6.12: Simulation run 3

6.2.4 Run 4

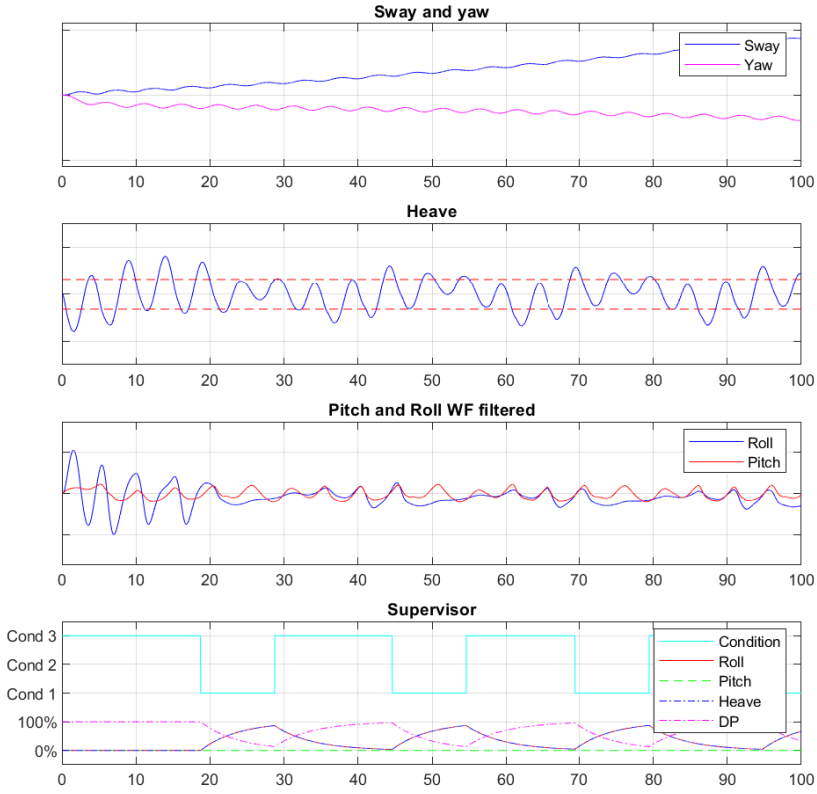

Figure 6.13: Simulation run 4

6.2.5 Run 5

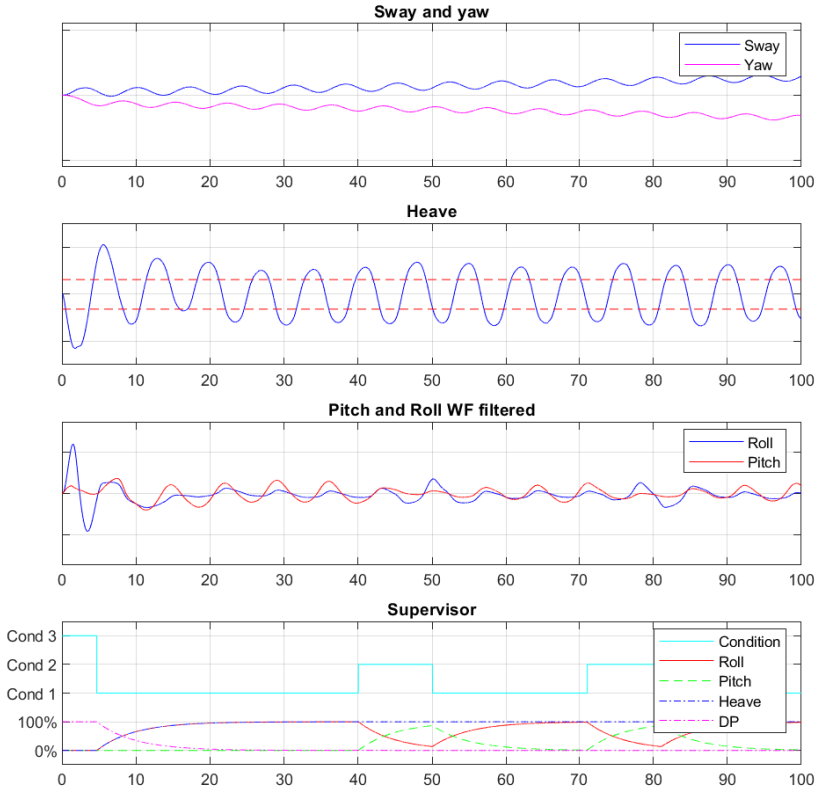

Figure 6.14: Simulation run 5

6.2.6 Run 6

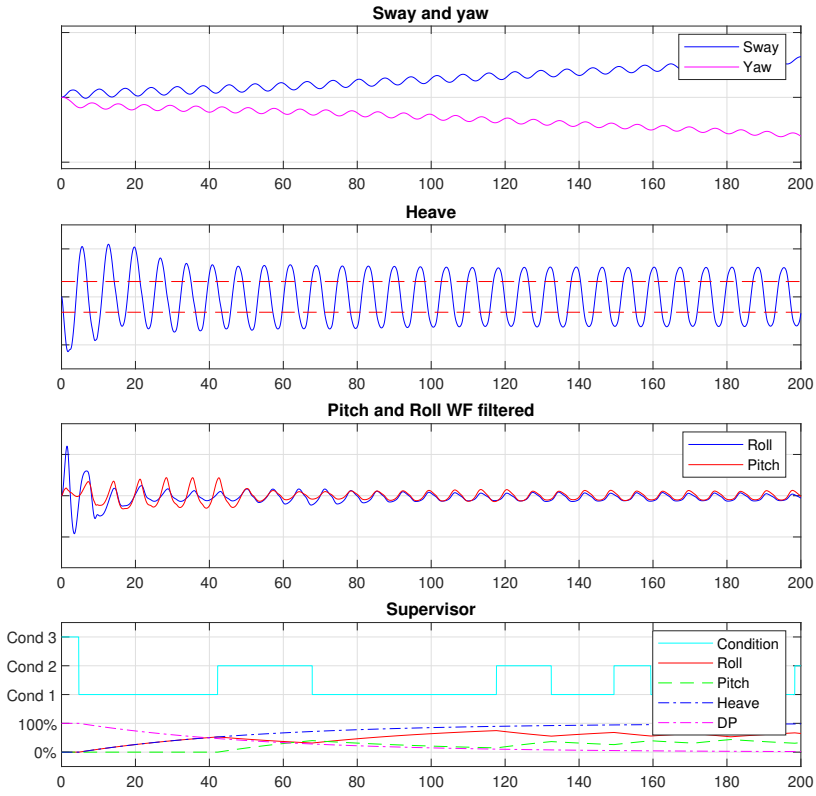

Figure 6.15: Simulation run 6

6.2.7 Run 7

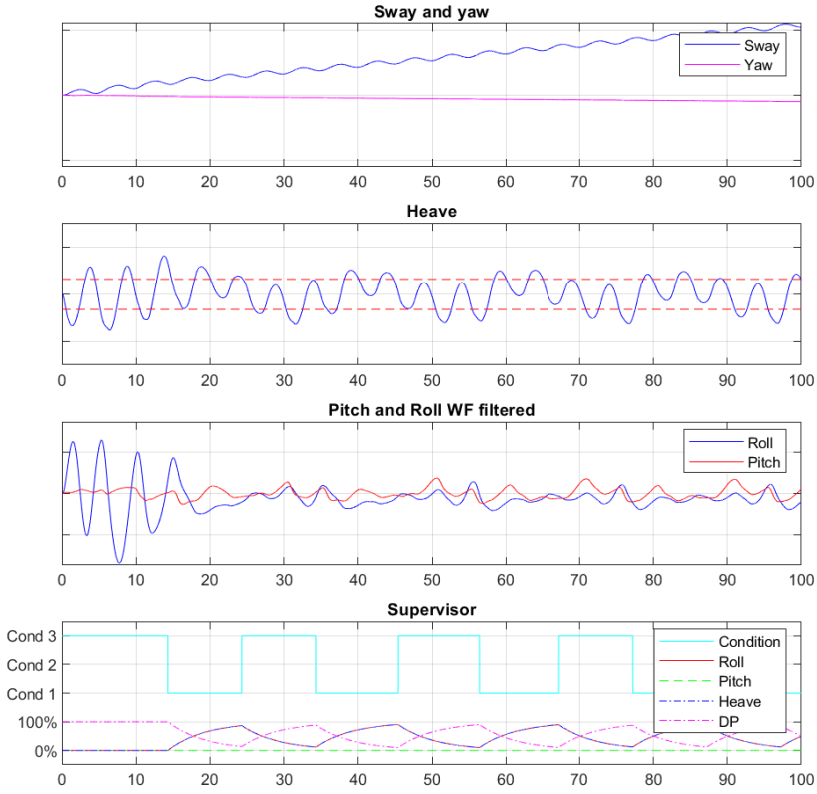

Figure 6.16: Simulation run 7

6.2.8 Run 8

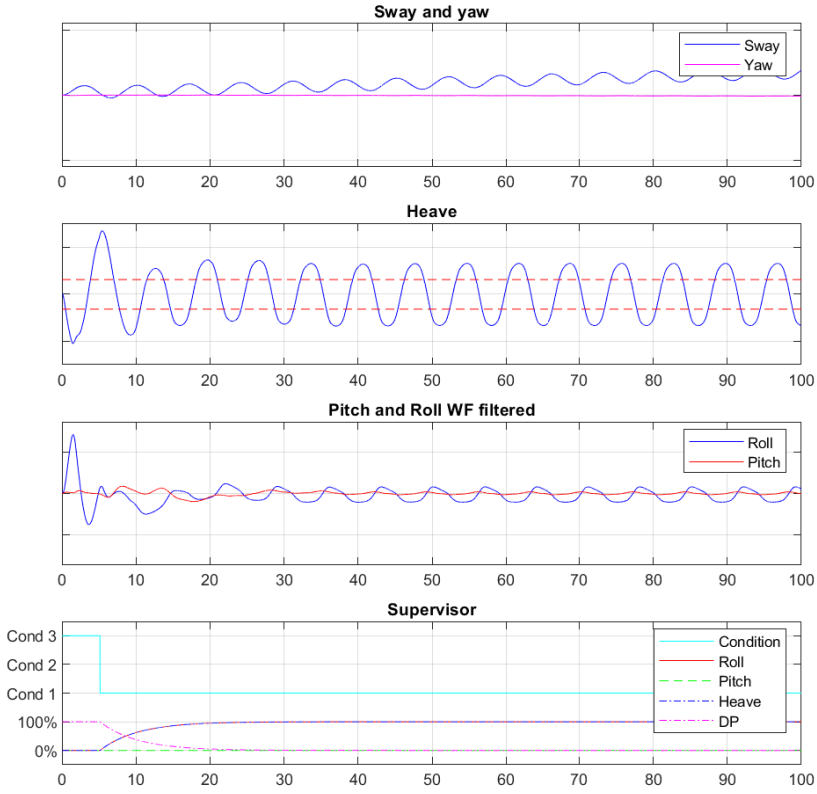

Figure 6.17: Simulation run 8

6.2.9 Run 9

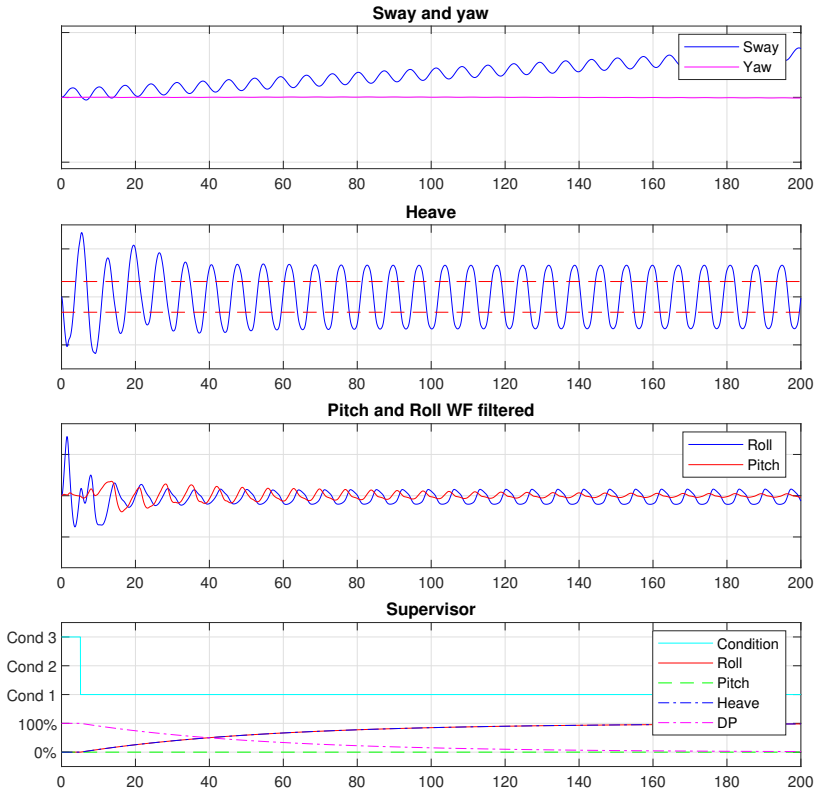

Figure 6.18: Simulation run 9

Chapter 7

Reviewing the simulation results

This chapter is dedicated to analysing the simulations results and identifying interesting behaviours.

7.1 Single cushion

7.1.1 0°sea

While the waves are travelling parallel to the vessels heading, they induce neither sway nor yaw moments and the system correctly allocates all available actuation to heave dampening.

7.1.2 45°sea

From the waves hitting the ship at 45°the supervisor quickly applies yaw control, but does not have sufficient actuation to work against the induced sway motions. This is similar to earlier results [Storvold (2018)], and can be attributed to actuator saturation. Still, in figure 6.5, from run 5, it is clear that the sway motion is significantly slowed by the vent valve thrust forces.

7.1.3 90°sea

When the waves are travelling normally to the ships heading they induce a large sway force that the actuators cannot match. The heading, however, is effectively controlled by the candidate controller, but remains in the condition border.

7.2 Split cushion

7.2.1 0°sea

The split cushion scenario provides a bit more interesting patterns in 0°sea. In Run 1 the heave and pitch dampening manages to get pitch RMS below the roll RMS and the supervisor uses all three conditions. In run number 2 and 3, the supervisor settles at the heave and pitch dampening controller.

7.2.2 45°sea

While in 45°seas, the vessel experiences both pitch and roll motion, and in 1,5m waves [6.13 manages to have well over 60% uptime on the DP controller. The DP system, however struggles with the same input saturation as the sway and yaw PID controllers. The latter runs, however shows how the system manages to balance roll and pitch while keeping heave dampening at 100%. In run 5, with fast controller changing, this happens in cycles, but in run 6, with a controller change slower than the conditions change, the σ value settles between predefined values. From looking at the roll and pitch plot, it is clear that the RMS values are in the area shown below in figure 7.1.

7.2.3 90°sea

In 90°sea, roll motion dominates, and the supervisor prioritises roll motion accordingly, but with the smaller wave allowing for some DP control activity.

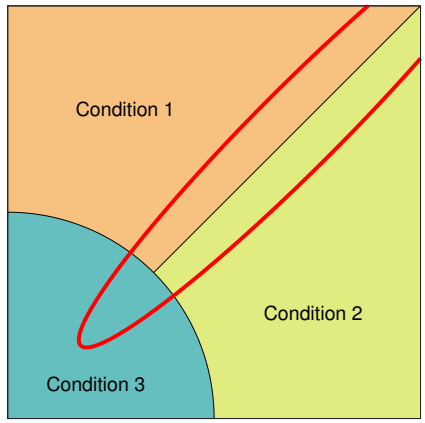

Figure 7.1: Conditions visualized in a 2D approximation

Chapter 8

Scale test setup

The scale tests were conducted at Sintef Ocean ”Havbassenget” lab, as part of a larger project including NTNU, Sintef and UMOE Mandal. The model testing revolved around a scale model of a proposed hull design for split cushion operation. Because of this all test results included in this thesis will be from the split cushion scenario.

8.1 Physical setup

The craft was fitted with five electrical lift fans, one for each of the four air cushions, plus one for the cushion separator. The lift fans were kept at a fixed RPM for the duration of each test. The vessel was attached to the sides of the facility by cables attacked to the basin sides by springs, the spring were selected as to only induce motions of frequencies well below the scope of the control systems. The facility, ”Havbassenget”, has a built in wave generator that was used to create disturbances in the form of either sinusoidal waves or more erratic randomised wave patterns.

8.2 Control and logging setup

The facility at Havbassenget has an optical positioning system that uses fixed cameras observing tracking elements mounted to the vessel. Measurements from this system, along with accelerometer from the vessel was provided to the control system at 200 Hz and logged at 100 Hz. The logged file also included amplitude measurements of waves passing the vessel, selected control system signals and vent valve positions.

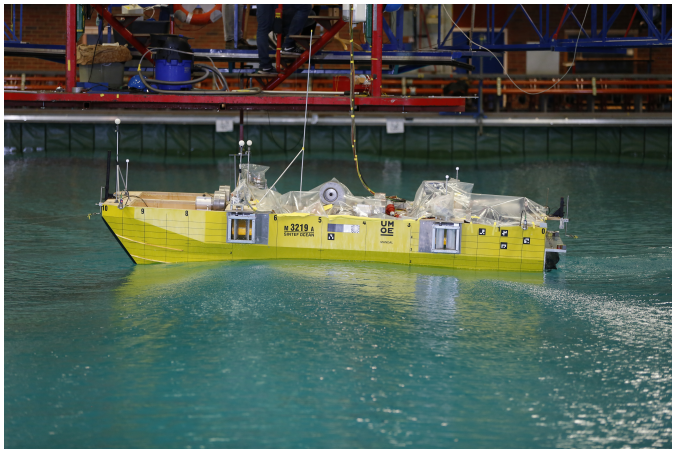

Figure 8.1: Sideview of the model vessel

Filtering, control and logging was all done through the Labview system, conversion of the code from this thesis' Matlab/Simulink work was done by Øvind Auestad of UMOE Mandal and verified by the author.

8.3 Controller parameters

As part of the project that initiated these model tests, all candidate controllers were trialed separately before the tests dedicated to hybrid control were conducted. As such, the tuning variables found during this testing could be reused as part of the hybrid control system.

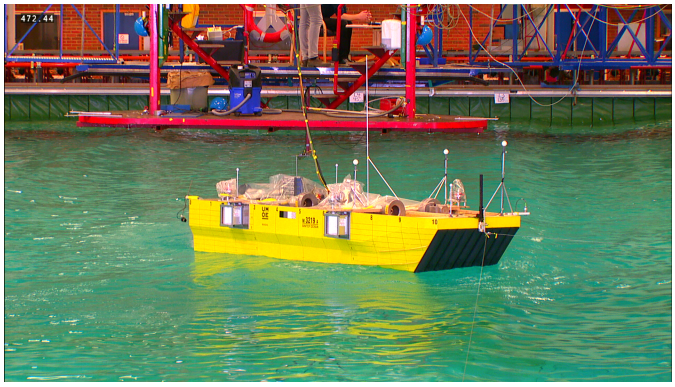

Figure 8.2: The model vessel in a diagonal orientation

Chapter 9

Scale test results

The scale test were only conducted for the split cushion scenario, in this chapter time series cut from the tests will be presented. The y axis of most plots are anonymised in order to protect UMOE Mandals interests. The time axis has been scaled to match the model scale, the same scaling was also applied to the waves generated by the wave generator.

Plot number	Wave direction	Wave height	Wave period	T_C
1	0°	2,5m	7s	5s
2	45°	2,5m	7s	5s
3	45°	1,5m	5s	5s
4	45°	2,5m	7s	50s
5	90°	1,5m	5s	5s

Table 9.1: Table of parameters

9.1 Exert 1

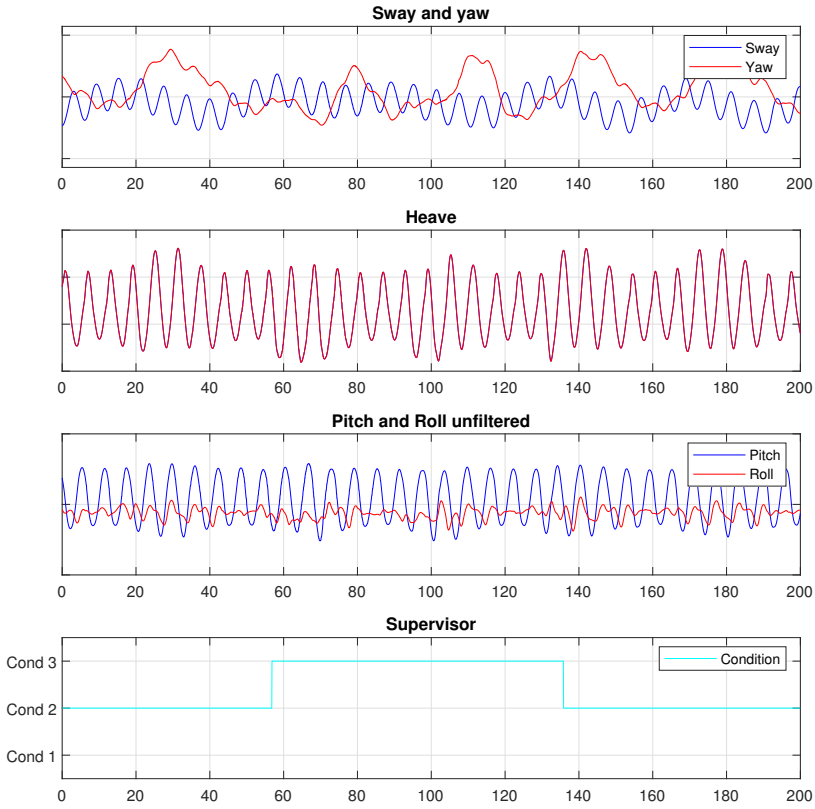

Figure 9.1: Model test exert 1

9.2 Exert 2

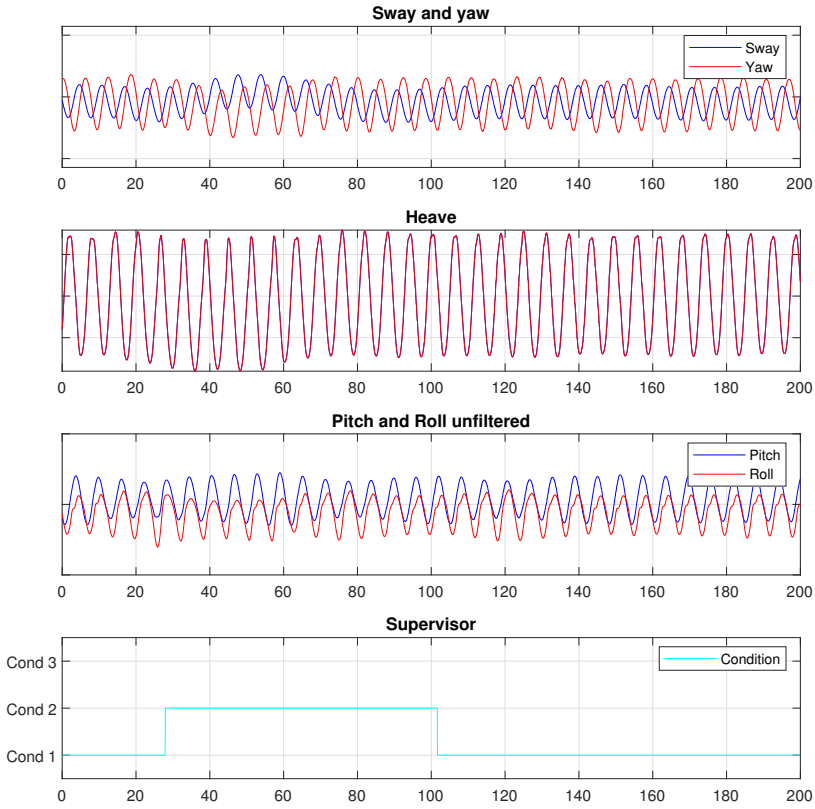

Figure 9.2: Model test exert 2

9.3 Exert 3

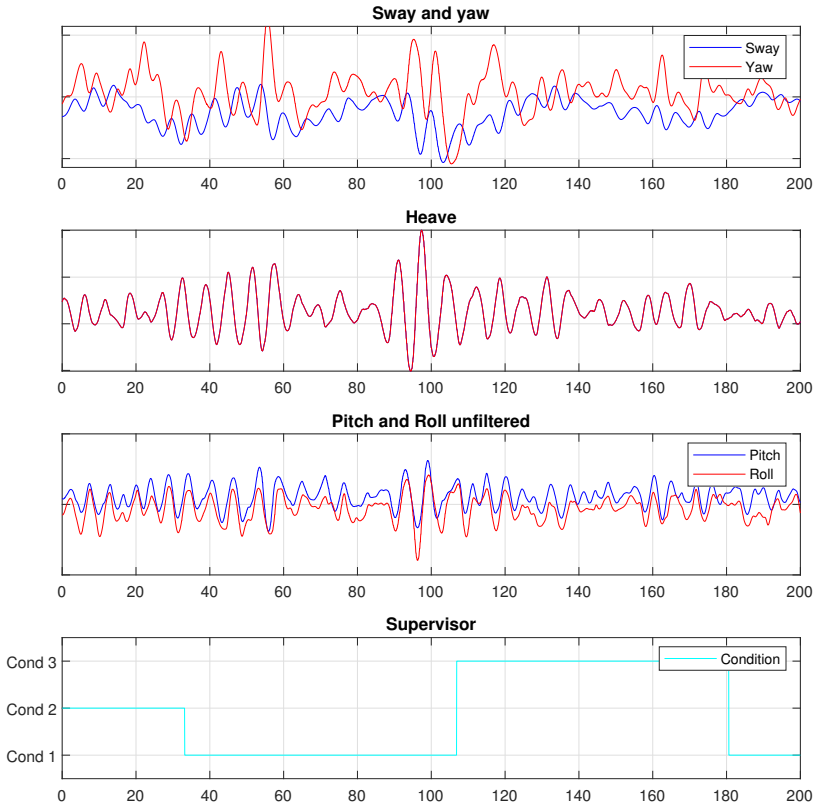

Figure 9.3: Model test exert 3

9.4 Exert 4

This exert shows the wave generator being turned off at about the 130s mark.

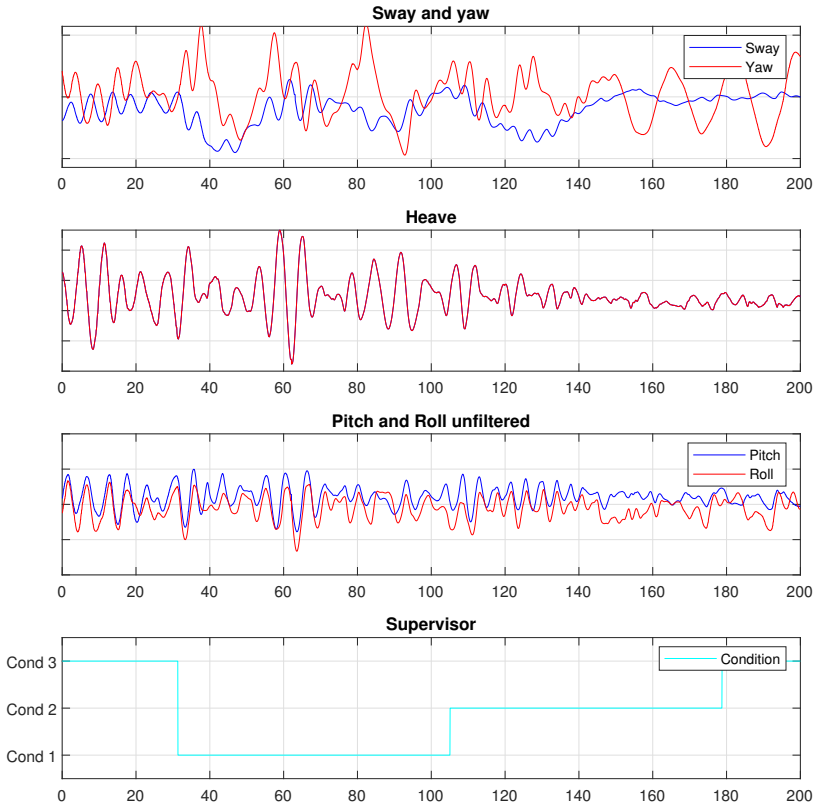

Figure 9.4: Model test exert 4

9.5 Exert 5

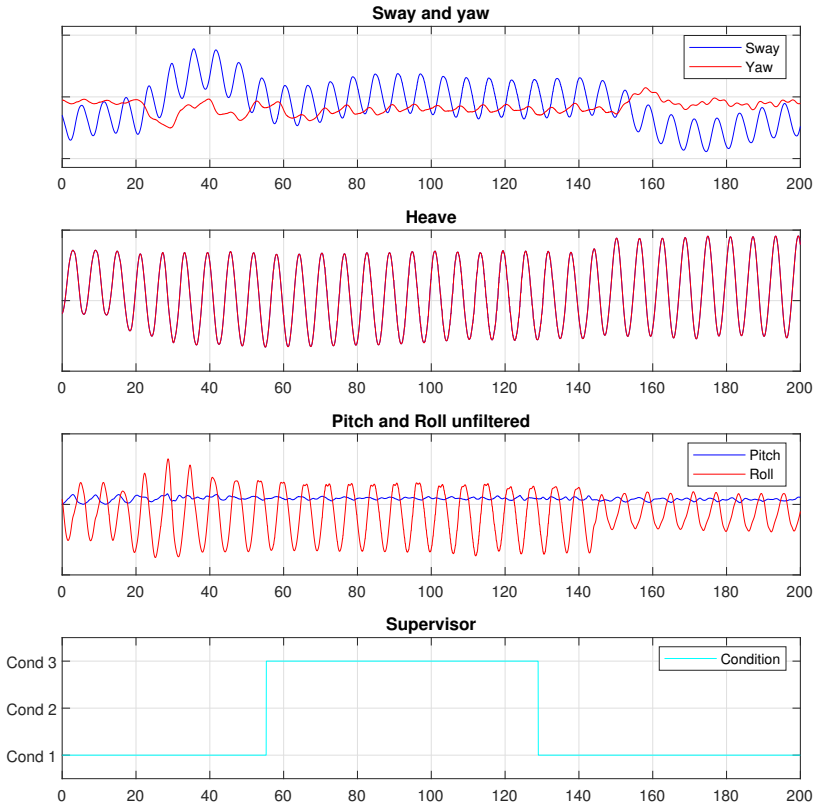

Figure 9.5: Model test exert 5

Chapter 10

Simulation and scale test comparisons

Due to the noisy nature of real life and especially model scale experiments, and a lower availability of measurements, not all the results from the previous chapter can be as easily interpreted. In this chapter, some of the identified behaviours from chapter 7 will be compared to their scale test counterparts.

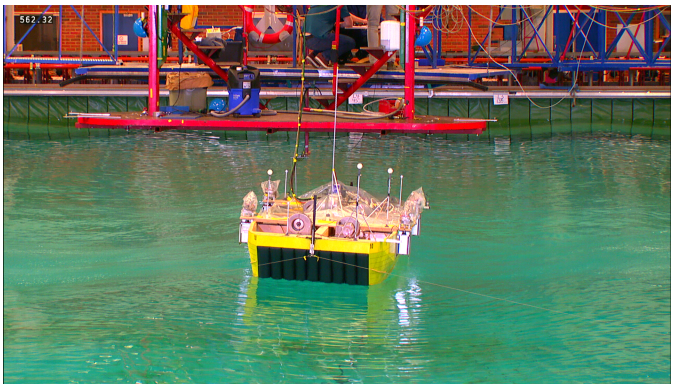

Figure 10.1: The model vessel with crossing waves

10.1 DP control

One of the larger mismatches between simulation and tests was that the DP system, when allocated to inputs, was able to return to the reference position and heading in exerts 3 and 5, and sway position only in exert 4. This was not present in the simulations where the system was input saturated even at smaller waves. It is clear that the simulation has some discrepancy in terms of the effects of waves on the vessel.

10.2 Roll and pitch control

The tendency for the supervisor to make slowly varying signals adhere to condition boundaries is replicated in the model tests. The tendency seems to be stronger when T_C is larger as can be seen in exerts 4. However, even in exert 2, where T_C is 5s, it is clear that the highest amplitude motion is prioritised.

10.3 Switching logic

The switching logic used as an example replicated its simulated behaviour in the model tests. In exert 5 the system stops heave dampening for a short while, but the dwell time ensures the VVDP system has a chance to return the vessel to its reference position before it is allowed to resume heave dampening. However some elements were not correctly scaled to model scale, resulting in an disadvantageous timing.

10.4 Heave damping

The heave motions in the model tests was a lot more erratic than in the simulations. This caused the slow pseudo RMS signal to not always catch when the heave motions should be dampened, this can be seen in the first exert. Other than that the heave dampening was less reliable than in the simulations, but overall just as effective.

10.5 General dynamics

One of the more obvious mismatches is the 50s periodic movements of the vessel in the model tests. These were not present in any of the simulation runs and might be due to the tethers responsible for keeping the vessel in the center of the basin.

Chapter 11

Conclusion and further work

11.1 Supervisory hybrid control

Supervisory control as presented in this thesis holds a number of advantages over more commonly used multiestimator versions as used by [Hespana (2002)]. Many of these advantages only exists when the system is being applied to MIMO, or at least MISO, systems.

It requires less modelling than multiestimator systems, making it possible to implement for very complex systems. It also makes it easier for a user to modify the system should the existing prioritisation not be as wanted.

The advantages of the simple modification also came into fruition when premade controllers were to be added. The user of the supervisory control system needed no insight into the inner workings of the candidate controllers in order to create condition and σ vector pairs that implemented the control inputs.

Some pitfalls did however show up when generating signals for the conditions. Some knowledge of the frequencies of motion in the system the conditions apply to should be taken into account. An example of how this can go wrong occurred when the pseudo RMS signal was incorrectly scaled down to model scale. This led the system to not pick up on faster varying heave amplitudes.

11.2 Hybrid control for Surface Effect Ships

Surface effect ships have proven to be a complex MIMO system where all inputs affect many states, even more so for the new split cushion design where all for inputs lead to five states. With the input saturation problems apparent in both this thesis and previous work [Storvold (2018)], controlling all five states at one would give each single controller significantly diminished effectiveness. As such a hybrid control system lets the vessels command and control system monitor all states and control those where control is wanted.

The example condition and σ pair used in this thesis were functional, and for the split cushion scenario provided a way to balance balance pitch and roll motions while awaiting calmer seas before prioritising positioning.

11.3 Timing and convergence

When $T_C << T_D$ the system will always reach a predefined controller setup, and this can be seen by some to be a safer option. However with $T_C >> T_D$ the system could settle on new controllers, as was seen with a heave, pitch and roll dampener in 45°sea. This was a positive change for that specific situation, but convergence to a constantly changing condition could give unforeseen results.

11.4 Further work

The easiest way to improve upon the hybrid control system in this thesis could be to simply create more condition and σ vector pair, or even just new candidate controllers. Further research into using more complex condition statements could also be conducted. These could be predictive, have integral or derivative elements, or ever be based of estimator errors as in [Hespana (2002)].

For the ship itself, it's largest weakness in terms of thrust control seems to be lack of thrust itself. A possibility might be to offload low frequency sway and yaw to tunnel thrusters while letting the existing system handle wave frequency components of the same signals.

As the system did well while in a configuration what mimicked adaptive control, a purely adaptive scheme for mixing control signals should be considered. It could be able to create any mix of controllers, all while having robust convergence proofs.

Bibliography

Auestad, 2012. Heave control system for a surface effect ship: Disturbance damping of wave induced motion at zero vessel speed. NTNU master thesis.

Auestad, O., T. Gravdahl, e. a., 2014. Motion compensation system for a free floating surface effect ship. Proceedings of the 19th World Congress The International Federation of Automatic Control.

Auestad, O., T. Gravdahl, e. a., 2015. Boarding control system for improved accessibility to offshore windturbines: Full-scale testing. Control Engineering Practice 45.

Bua, N. H., Vamråk, V. M., 2016. Sway control on a surface effect ship. NTNU Departement of Marine Technology Master Thesis.

Clark, Dennis J., e. a., 2011. The quest for speed at sea. CARDEROCK DIVISION, NSWC — TECHNICAL DIGEST.

Fossen, T., 2011. Handbook of Marine Craft Hydrodynamics and Motion Control. John Wiley & Sons.

Fossen, T. I., Perez, T., 1998. Kalman filtering for positioning and heading control of ships and offshore rigs. IEEE.

Fossen, T. I., Perez, T., 2004. Marine Systems Simulator (MSS). `URL:https://github.com/cybergalactic/MSS`, [Online; accessed Aug 2018].

Hespana, J. P., 2002. Tutorial on supervisory control. Dept. Electrical & Computer Engineering, Univ. of California.

IMO, 2019. Guidelines on fatigue. [MSC.1/Circ.1598 24 January 2019].

J. Adams, A. W. Ernest, J. H. L., 1983. Design, development and testing of a prototype digital ride control system for surface effect ship part viii: Test on xr-1e ses. National Technical Information Service.

Kaplan, P., 1981. Dynamics and hydrodynamics of surface-effect ships. SNAME Vol 89, 211–247.

Lavis, David R., e. a., 1998. 40 plus years of acv development. Canadian Air Cushion Technology Society.

Lavis, David R., S. K. B. j., 1991. Surface effect ship (ses) developments worldwide. Naval Engineers Journal.

Storvold, H., 2018. Multivariable ses control: Using linear mixing. NTNU Project Report.

Sørensen, A. J., 1995. Design of ride control system for surface effect ships using dissipative control. Automatica Vol 31, 183–199.

UMOE-Mandal, 2019. MAROFF SES service fartøy - NUMERICAL SIMULATOR FOR THE MOTION CONTROL SYSTEM. [Umoe Mandal Internal Document].

WMO, 2018. Manual on Codes - International Codes, Volume I.1, Annex II to the WMO Technical Regulations: part A- Alphanumeric Codes. [Online; accessed March 2019].

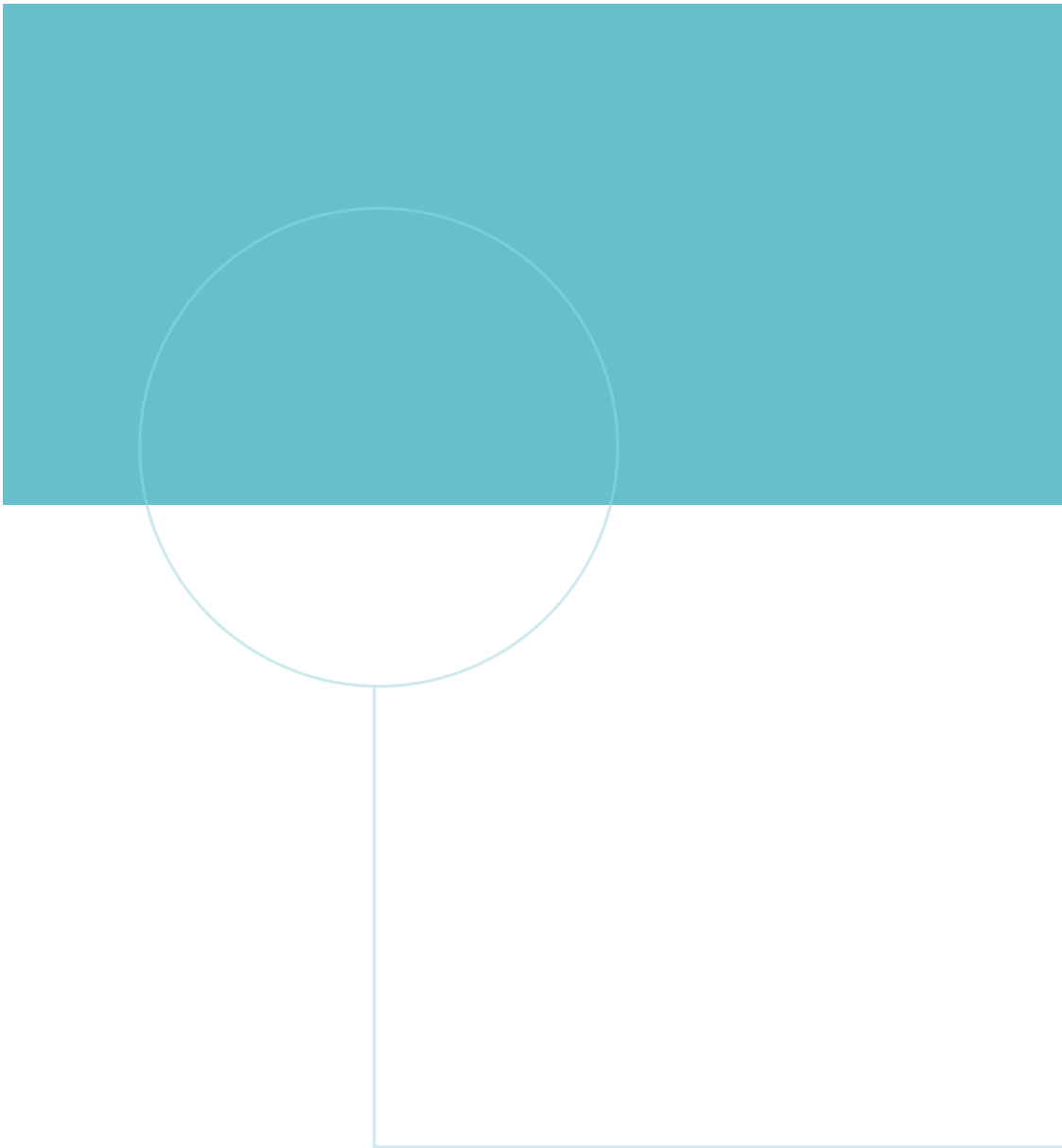

NTNU
Norwegian University of
Science and Technology